LA-UR-08-03993

Use of a Collocated Sensor/Actuator for Dynamic Control and Structural Health Monitoring

Molly Nelis[1], Kenneth Ogorzalek[2], Alberto Vázquez Ramos[3], Gyuhae Park[4]

[1] Department of Electrical & Computer Eng. and Department of Mechanical Eng., Rose-Hulman Inst. Technology, Terre Haute, IN 47803
[2] Department of Civil Eng. and Mechanics, University of Wisconsin-Milwaukee, Milwaukee, WI 53201
[3] Department of Mechanical Eng., University of Turabo, Gurabo, PR 00787
[4] The Engineering Institute, Los Alamos National Laboratory, Los Alamos, NM 87545

ABSTRACT

This paper presents the dual use of a piezoelectric self-sensing actuator for both vibration suppression and structural health monitoring (SHM) applications. For vibration suppression, positive position feedback is used for control, where the impedance method or time series autoregressive models are utilized for structural damage detection in SHM. For this approach, only a single piezoelectric transducers element is employed to reduce the number of system components, while enhancing the structural performance. To validate this technique, an analytical model is first developed using the basic principles of PZT materials and the Euler-Bernoulli beam theory. This analytical model is then experimentally verified on a cantilever beam and a three story bolted structure. This paper summarizes considerations needed to design such systems, techniques for control and signal processing, experimental procedures and results, as well as additional issues that can be used as a guideline for future investigations.

Key words: Piezoelectric Materials; Self-Sensing Actuation; Vibration Suppression; Structural Health Monitoring; Positive Position Feedback

1 INTRODUCTION

1.1 Background

Using piezoelectric (PZT) materials has become widely accepted for structural control applications. The use of PZT actuators to control structural vibrations was explored by Crawley et al. (1987) [1]. Positive position feedback was first used for vibration control by Fanson et al. (1990) [2]. This method allowed for several modes to be controlled simultaneously. With recent advances in this field, sensing and actuating have been combined into a single element, a self-sensing actuator, thereby allowing for enhanced capabilities and reduced spillover-effects. In utilizing a self-sensing actuator, which was described by Dosch et al. (1992) [3], the single element reduces the number of system components and decreases the instrumentation by half. Weight and cost are also decreased by using one component versus two.

Tani et al. (1997) [4] brought up some issues with collocated control, including temperature sensitivity and issues associated with the use of simplified PZT models employed in existing studies. It is possible to compensate for these errors digitally like Okugawa et al. (2002) [5] or by using analog components like Simmers et al. (2004) [6, 7]. A bridge circuit, similar to the one used by [6], is used within this paper to distinguish the control voltage from the sensing voltage.

Very little work has explored using self-sensing PZT sensors for structural health monitoring (SHM). Castillo et al. (1999) [8] used collocated sensors to detect damage, but found difficulties in detecting location and extent of the damage. The point impedance method has been used with collocated sensors to detect damage Chaudhry et al. (1995) [9] and the recent work was summarized by Park et al. (2003) [10].

When combining a sensor and an actuator into a single self-sensing actuator, controlling vibrations is the primary objective, as the single element decreases the weight and system cost, while increasing instrumentation efficiency. Recently, numerous researches have addressed and improved the ability for self sensing. However and in light of the recent I-35W bridge collapse in Minneapolis, there is an urgent need to also effectively and efficiently monitor structural health. Visual inspection is the predominant method for assessing structural health, yet this technique is often affected by the working environment and access restraints. Therefore, there is a need for an effective tool that can suppress unwanted vibrations while safely inspecting the structure.

This paper investigates the use of a single PZT self-sensing actuator for SHM applications. This paper will also analytically and experimentally investigate the effects of an unbalanced bridge circuit in relation to SHM as well as vibration suppression. For structural health monitoring, the time series autoregressive (AR) model and the correlation between frequency response functions (FRF).

2.0 CIRCUIT AND STRUCTURE MODELING

2.1 Bridge Circuit

As an important component for effectively utilizing the self-sensing actuator, a bridge circuit is used to separate the input voltage from the sensing voltage, where a self-sensing actuator is placed in parallel with capacitance that is matched to the self-sensing actuator. The following figure displays the electrical configuration used within this paper, as the self-sensing actuator (PZT patch) is imbedded into the bridge circuit.

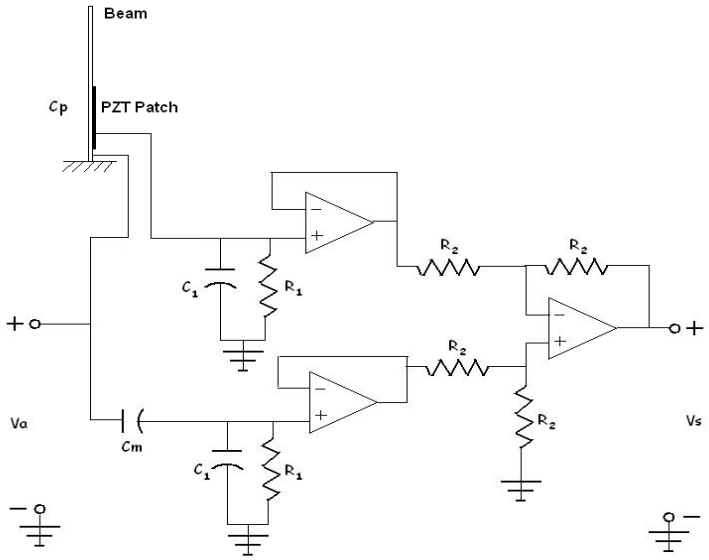

Figure 1. Bridge Circuit with Self-Sensing Actuator

In Figure 1, Va is the input voltage, Vs is the output sensing voltage, Cp is the PZT patch capacitance, and Cm is the matched capacitance. Because the input voltage displays a higher magnitude than the output sensing voltage, the bridge circuit is required to distinguish the two voltages from one another and to allow for an efficient way to suppress structural vibrations and detect damage imposed on a structure.

2.2 Analytical Model

Using linear superposition, it is possible to model the bridge circuit and PZT patch as the sum of two single source circuits, where Zp, Zm, and Zeq are the PZT patch impedances, matched capacitance, and signal conditioner, respectively.

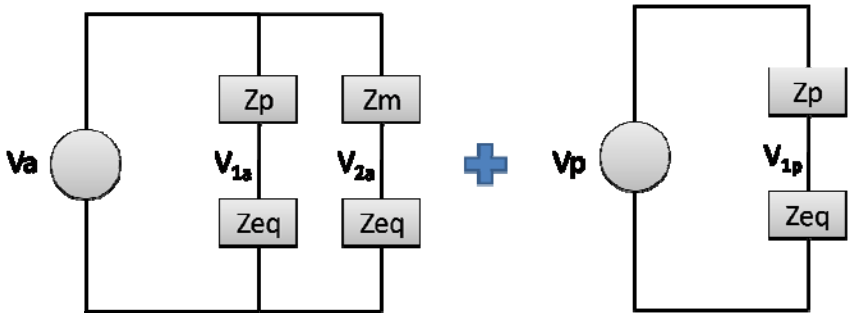

Figure 2. Bridge Circuit with Equivalent Impedances

The circuit provided in Figure 1 is split into two systems, one where Va is the source and one where Vp is the source. The simplified bridge circuit is displayed in Figure 2, where the components are modeled in the impedance domain. For the Va superposition circuit, matched capacitance is utilized. However, matched capacitance is not used in the Vp superposition circuit. The voltages V1a and V2a are solved in the Va circuit, and V1p is solved in the Vp circuit. If Zp and Zm are equal, then the sum of the voltages will only be V1p. The sensor voltage (Vs) is therefore defined as the sum of the simplified bridge circuit:

$$Vs = V1a - V2a + V1p$$

In order to validate the equivalent impedance circuit, an analytical model is comprised in Simulink. The model was altered to investigate the bridge circuit dynamic characteristics and the self-sensing system stability.

3.0 DYNAMIC CHARACTERISTICS OF BRIDGE CIRCUIT

Before the bridge circuit can be efficiently implemented, the bridge circuit dynamic characteristics were investigated through modification of the matched capacitance in comparison to the PZT capacitance. The experimental setup was configured as the bridge circuit represented in Figure 1. Within the experimental setup, a cantilever aluminum beam is used as a real life structure with the following material properties:

Cantilever Beam	
Length	223 mm
Width	37.9 mm
Thickness	1.13 mm
E	6.9 e^{10} Pa
Mass Density	2700 kg/m^3

Table 1. Properties of Cantilever Beam with PZT patch

PZT patch PSI 5A4E (5A), which is often compared with PSI 5H4E (5H) PZT patch, is mounted on the top of the cantilever beam for determining the bridge circuit dynamics characteristics. The patch has custom dimensions of 72.4 x 33.0 x 0.27 mm^3. In using piezoelectric materials, these materials are highly sensitive to temperature change, as there is a 1% change in PZT capacitance for every 5.5 °C change in a 5A PZT with dimensions of 70 x 10 x 0.1 mm^3 [6]. Although the dimensions from [6] are not consistent with the dimensions used in this study, the general concept of patch 5A being less temperature sensitive than patch 5H is apparent. Therefore, PZT patch 5A is used for the experimental test. The configuration is displayed in the following figure.

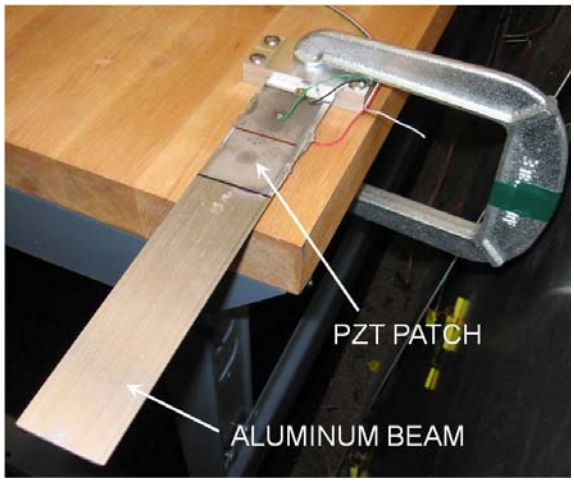

Figure 3. Experimental Setup of Cantilever Beam and PZT Patch for Determining the Dynamic Characteristics of Bridge Circuit

The material properties and patch location of the mounted PZT patch is provided in the following table:

PZT Patch	
Length	72.4 mm
Width	33.0 mm
Thickness	0.27 mm
E	5.2 e^{10} Pa
Experimental Capacitance	135 nF
Strain Coefficient	-190 e^{-12}
Voltage Coefficient	-11.6 e^{-3}
Permeability	8.9 e^{-12} F/m
Distance from Support to Patch	9 mm

Table 2. Properties of PZT Patch

3.1 TEMPERATURE CHARACTERISTICS OF BRIDGE CIRCUIT

Ideally, the optimal situation for maintaining a stable bridge circuit is to have Cp = Cm. Often times this is quite challenging, as temperature variance can impose significant changes to the PZT material properties. Therefore, the effects of varying capacitances where investigated. When Cp > Cm, the frequency response function displays resonance before anti-resonance for a given mode. The pattern is characteristic of a stable circuit and indicates that the patch will provide reliable data. However, if Cp < Cm, the bridge circuit is unstable and results in defective data. For this situation, anti-resonance occurs before resonance for a given mode within the FRF, as is shown in the following figures.

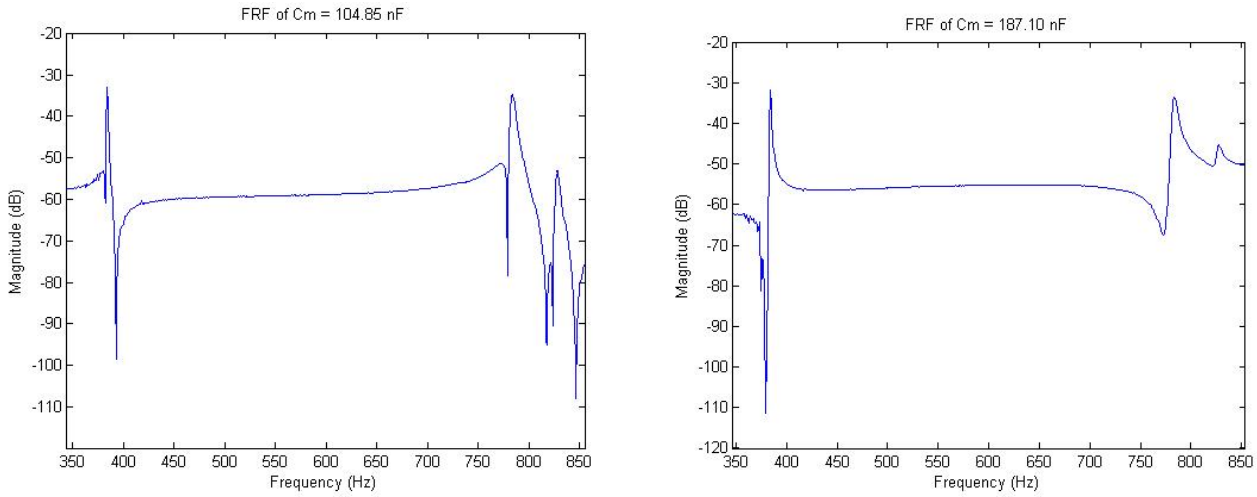

(a) (b)

Figure 4. Experimental FRF Plots of (a) Stable Bridge Circuit (b) Unstable Bridge Circuit

It is noteworthy to mention that the FRF in the previous figure does not recognize the second natural frequency for the cantilever beam. This observation is most likely because the PZT patch is located at a node point for the second mode shape.

Analytical and Experimental Natural Frequencies for PZT Patch in Hz					
Mode	1	2	3	4	5
Calc.	30	116	326	639	1060
Exp.	28.7	119	384	781	825

Table 3 comparing natural frequencies of analytical and Experimental results for MFC Patch

To validate the experimental data, the following figure represents a Simulink model for determining whether or not the bridge circuit is stable.

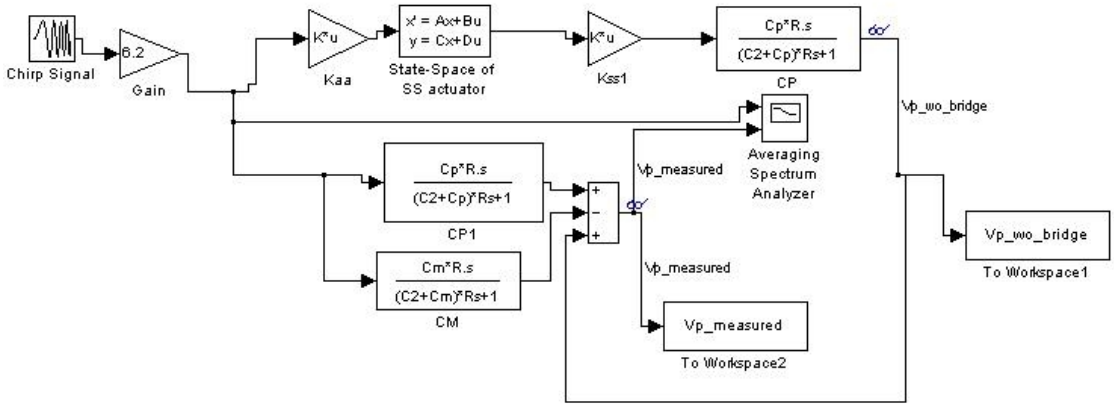

Figure 5. Simulink Model of Bridge Circuit for Analytical Model

The matched capacitance values for the analytical model were modified in correlation with the experimental capacitances. Under these circumstances, the patterns of instability were comparable to the experimental FRFs, which are displayed in the following diagrams:

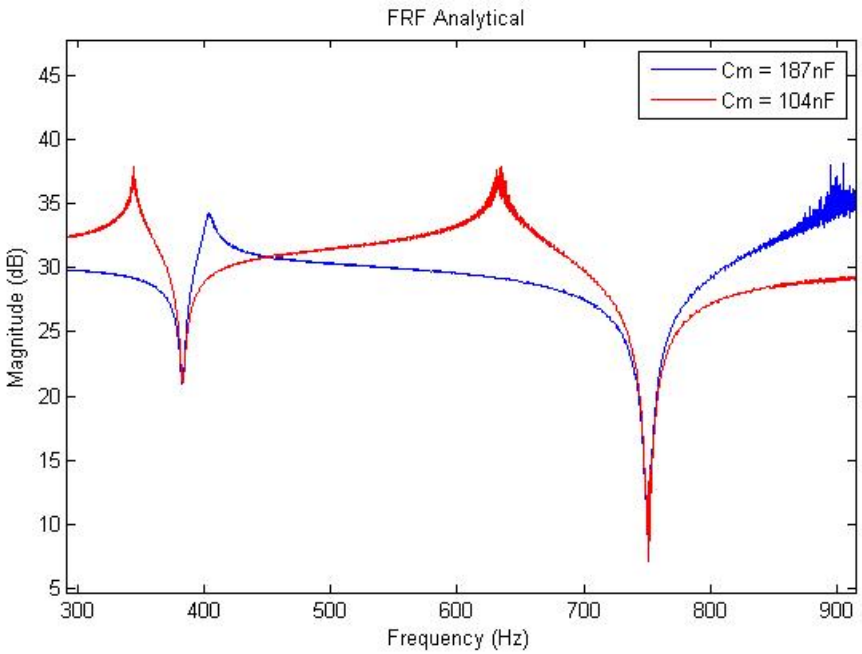

Figure 6. Analytical FRF Plots of a Stable and Unstable Bridge Circuit

With the known FRF patterns for a given matched capacitance, these dynamic characteristics are used in future tests for determining whether or not the bridge circuit is stable or unstable within different electrical configurations.

3.2 VIBRATION SUPPRESION USING MFC PATCH

Due the difficulty of detecting the second mode, a second PZT patch cantilever beam (MFC beam) system was fabricated for the remainder of the testing. Table 4 and Table 5 display the aluminum beam and PZT patch material properties, respectively:

Cantilever Beam for MFC	
Length	171.5 mm
Width	38.0 mm
Thickness	1.28 mm
E	6.9 e^{10} Pa
Mass Density	2700 kg/m^3

Table 4. Properties of Cantilevered Beam with MFC patch

MFC PZT Patch	
Length	6.34 mm
Width	14.0 mm
Thickness	0.30 mm
E	30.3 GPa
Experimental Capacitance	22.0 nF
Strain Coefficient	-170 e^{-12}

Voltage Coefficient	$-11.6\ e^{-3}$
Permeability	$8.90\ e^{-12}$ F/m
Distance from Support to Patch	22.0 mm

Table 5. Properties of MFC Patch

By modifying the analytical model properties, we were able to calculate the theoretical natural frequencies of the MFC beam and compare it to the experimental results as seen in Table 6.

Analytical and Experimental Natural Frequency Results for MFC Patch in Hz															
Mode	1	2	3	4	5	6	7	8	9	10	11	12	13	14	15
Calc.	33.2	208	583	1140	1890	2820	3940	5240	6730	8410	10.3k	12.3k	14.6k	17.0k	19.6k
Exp.	35.2	211	609	1210	1780	3000	4170	5770	6290	9211	9810	11.6k	14.4k	16.7k	19.7k

Table 6. Comparison of Natural Frequencies between Analytical and Experimental Models for MFC Patch

It is possible with the MFC patches to achieve vibration reduction to 20% of the original value. The PPF filter is tuned using an input sine wave at the first natural frequency. The filter damping value and gain are increased until a desired performance is reached. The non-MFC patch could only achieve vibration reduction of about 25% of the excitation. As seen in Figure 7, within 0.5 sec, the displacement magnitude decreases from 22.1 µV to 3.94 µV.

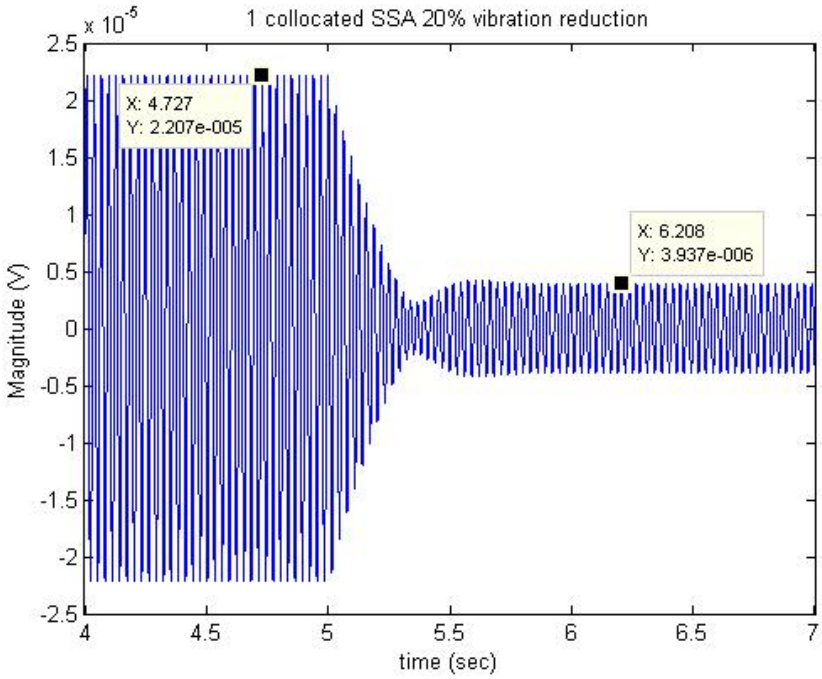

Figure 7. Vibration Suppression of Cantilever Beam

Using PPF to suppress the vibration due to an impact, it is clear that there is significant improvement in the beam settling time for the separate sensor and actuator system. In Figure 8 (a), the uncontrolled output sensor voltage experimental result has a settling time of 2.38 seconds. In Figure 8 (b), which consists of the controller being on, the output voltage has a settling time of 0.44 seconds. For Figure 8 (a) and (b), the settling times range from 75% of the maximum voltage to 25% of the maximum voltage.

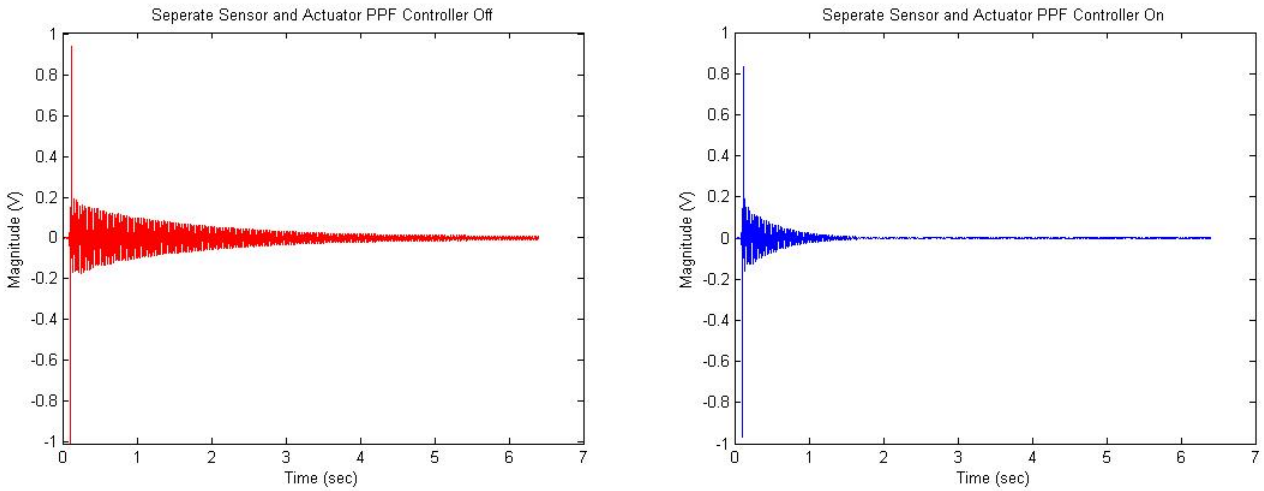

(a) (b)

Figure 8. Experimental Results of Separate Sensor and Actuator (a) PPF Controller Off (b) PPF Controller On

The self sensing actuator has similar performance to the separate sensor actuator. With the controller off, the output response settles in 1.92 seconds. However, when the PPF controller is on, the response has a settling time of 0.53 seconds. Because the gain on the PPF controller was decreased to maintain stability, the impulse was larger for the self-sensor. Therefore, it is expected for that the settling time for the self-sensor is longer than the separate sensor and actuator experiment. This phenomenon is seen in Figure 9 (a), the uncontrolled response, and in Figure 9 (b), the controlled for the self-sensor.

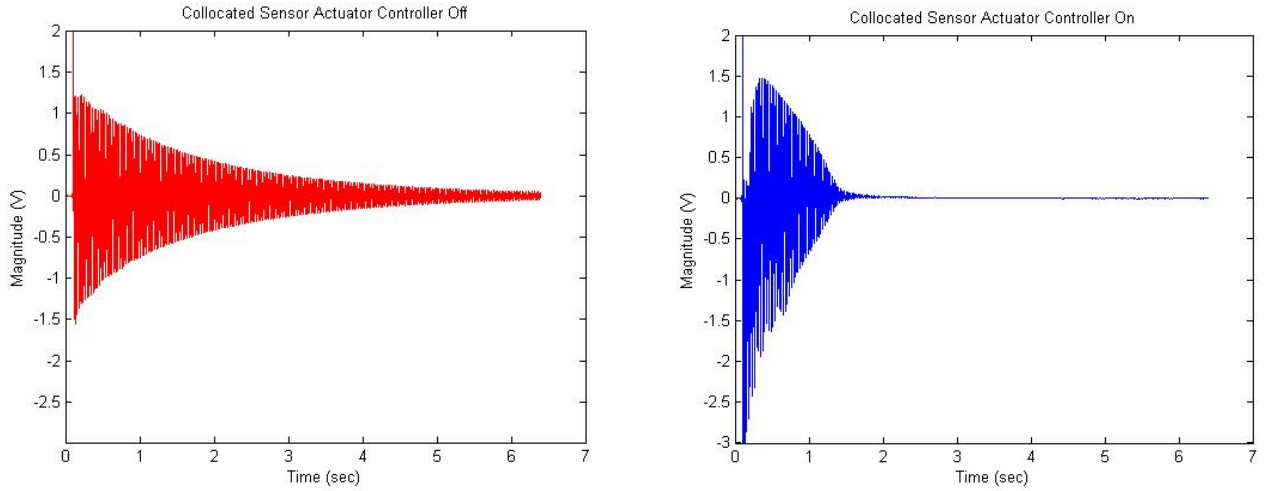

(a) (b)

Figure 9. Experimental Results of Collocated Sensor Actuator (a) PPF Controller Off (b) PPF Controller On

4.0 IMPROVING PERFORMANCE OF SELF-SENSING ACTUATOR SYSTEM

There are 2 significant problems with self sensors, temperature dependence, and frequency dependence. This group explored a method to increase the temperature of the bridge circuit used in vibration suppression, and designed a simplified circuit for the SHM sampling.

4.1 IMPROVING SELF-SENSING ACTUATOR TEMPERATURE STABILITY

To increase the self-sensing actuator system stability performance, multiple structures, PZT patches, and circuit configurations were investigated. In the first configuration, two PZT patches (MFC) are mounted onto an aluminum cantilever beam that is 171.5 x 38 x 1.28 mm^3. There are four bolts that secure two aluminum plates, thereby fixing the end of the cantilever beam. One PZT patch is located on the top surface of the beam while the other patch is mounted on the bottom surface of the beam (Figure 10). The intent behind this configuration is to have both patches impulse in a unimorph manner. However, this configuration induces challenge as the impulses from the two patches interfere destructively, thereby making it difficult to establish a sensing voltage.

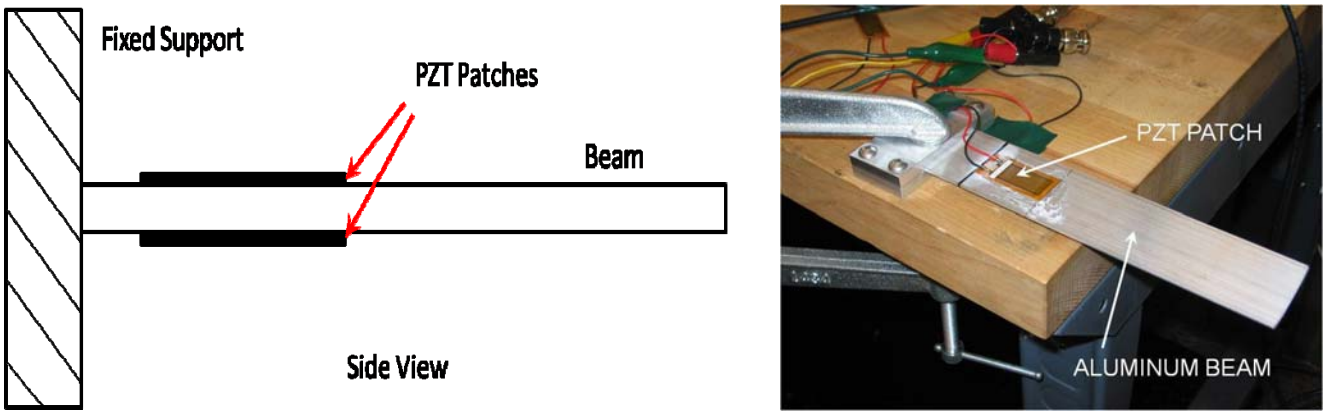

Figure 10. MFC Cantilever Beam (a) Side View (b) Experimental Setup

To distinguish a sensing voltage, this paper describes a novel idea of using two PZT patches that consist of different sizes and thicknesses and are positioned on the same side of the cantilever beam, which is addressed as the second configuration. Therefore, when inducing an input voltage, the voltages produced by the patches will vary in magnitude and can be subtracted from one another to display a sensing voltage. This novel idea allows for a bimorph rather than a unimorph behavior. Figure 11 illustrates the cantilever beam with two PZT patches of different physical properties.

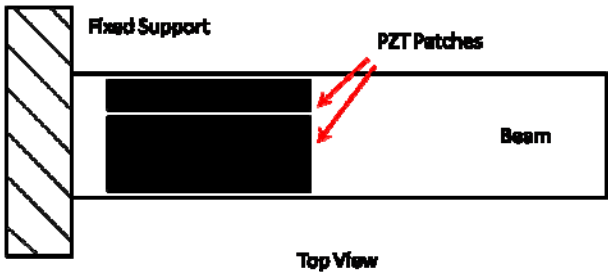

Figure 11. PZT Patch Configuration with Bimorph Characteristics

For the second configuration, the two patch areas are intentionally altered from one another. Therefore, from the definition of PZT capacitance for a parallel plate capacitor:

$$Cp = \frac{\varepsilon \cdot A}{t}$$

where Cp is the PZT patch capacitance, ε is the permittivity of the dielectric material, and A and t are the PZT patch area and thickness, respectively. From the definition of PZT capacitance, the PZT patch areas are held constant, thereby allowing for the PZT patch thickness to vary in order to accommodate the matched capacitance between the two patches. In using different size PZT patches, it is difficult to achieve a perfect matched capacitance for both patches. Therefore, a single patch will be attached to an external capacitor that contains a

small capacitance. This configuration will allow for a sufficient matched capacitance between the PZT patches, where the external capacitor does not affect the capacitance as the temperature varies.

While the bimorph configuration of the PZT patches was not verified experimentally due to time constraints, the unimorph configuration is not effective for low frequency excitation needed for vibration suppression. If tested, the different patches will produce different sensing voltages for the same excitation voltage. When the voltage from one patch is subtracted from another, the overall sensing voltage will be smaller than a single self-sensor patch. However the sensing voltage will be immune to temperature variation in this configuration.

4.2 SIMPLIFYING SHM SELF-SENSING ACTUATOR CIRCUIT

It is possible to simplify the circuit design used for SHM. By utilizing a capacitive voltage divider, the analysis is less complex and no longer dependent on frequencies from 0 Hz to 20 kHz. The change in performance between the self-sensor and the separate sensor and actuator is acceptable for SHM. Below in Figure 12 (a) are the experimental self sensor input performance (dashed line) and the actuator in the two patch system (solid line). As indicated in Figure 12 (a), there are slight differences between the two responses. In Figure 12 (b), the self-sensor output performance is displayed as the dashed line, while the sensor in the two patch system is the solid line. Even though the output responses are not identical, the self-sensor data is not compared to the separate sensor and actuator data when SHM is performed.

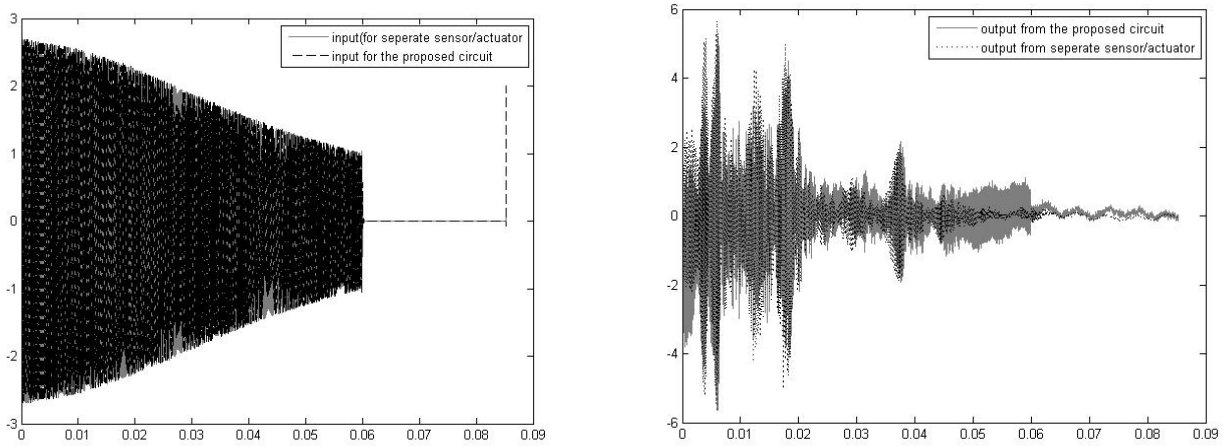

(a) (b)

Figure 12. Comparison of CSSA and Separate SA Time Series Data (a) Input (b) Output

5.0 STRUCTURAL HEALTH MONITORING

Two different methods were used to detect damage in the structure, frequency analysis and the time domain AR model. There is a clear shift in the time response data between the undamaged and damaged states. By implementing a statistical damage detection method on the error between the two types, it is possible to easily categorize structures.

5.1 SHM WITH SEPEARTE SENSOR AND ACTUATOR

For the initial damage detection exploration, the MFC beam previously mentioned is used, where damage is implemented by removing one of the four bolts used within the fixed support. A system model was made in Simulink. There is no correlation between the analytical model time responses and the experimental data. The magnitude was much smaller than the actual system response. As shown in Figure 13, the natural frequencies correlate fairly well between the analytical model and the experimental data, as there are slight shifts between the two. However, the frequency response functions between the analytical model and the experimental data do not

correlate well with each other. This effect may be due to an insufficient excitation voltage in the model, or damping which is too low.

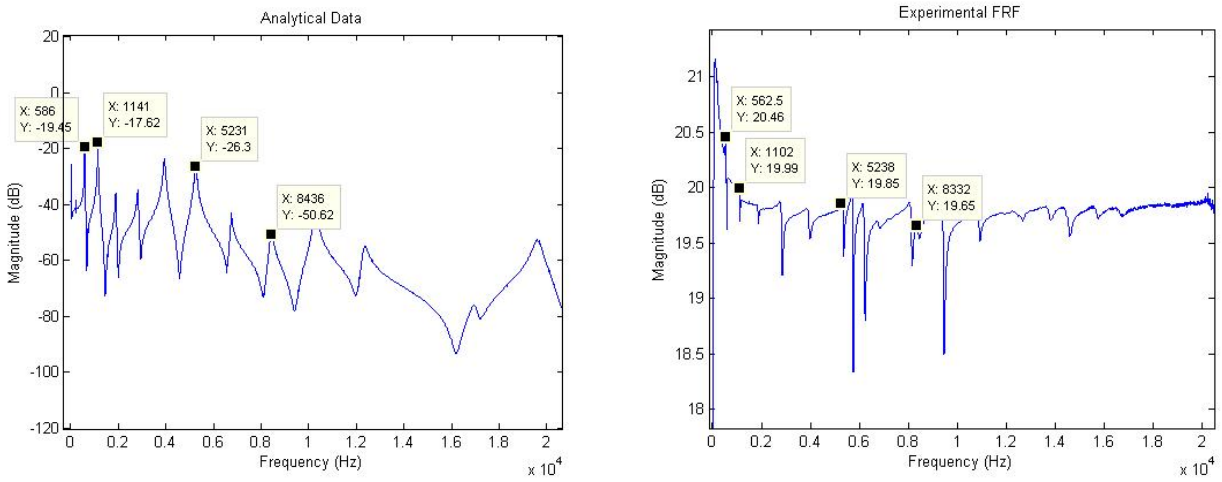

Figure 13. (a) Analytical FRF (b) Experimental FRF

There were two different statistical methods to analyze the AR model results, Principle Component Analysis (PCA) of the AR coefficients and an error vector method with a control limit at a 95% confidence interval. In PCA, the first 2 components are plotted, and the undamaged points will group around one value while the damaged group around another. When enough data is collected, a dividing line can be defined for a supervised SHM system. In Figure 14, the undamaged cases are marked with circles and the damaged cases are marked with crosses. As shown in the following figure, there is a clear distinction between the damaged and undamaged cases.

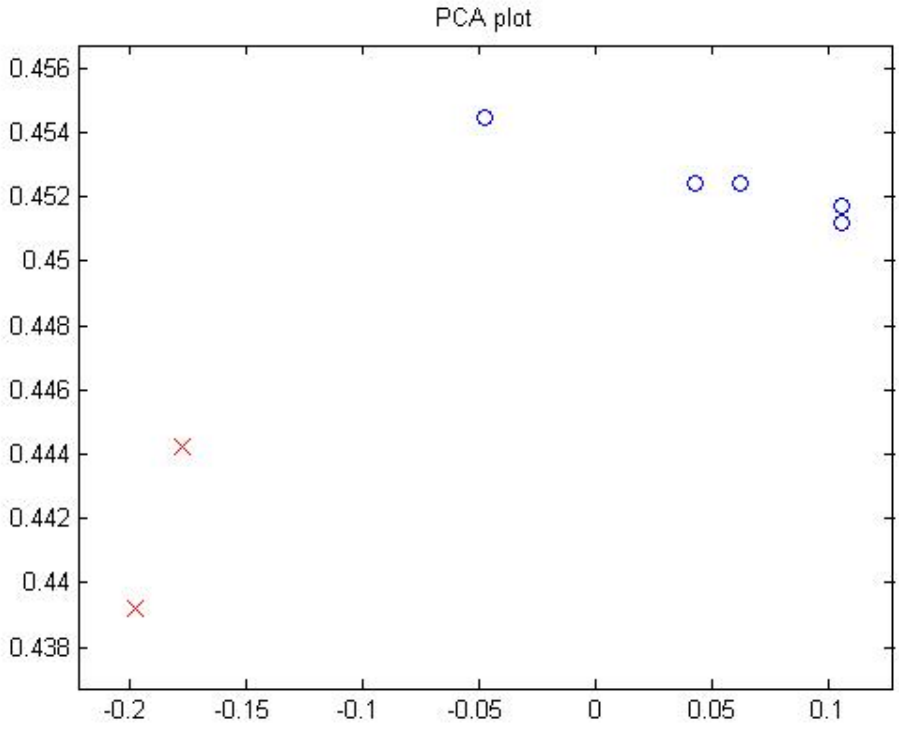

Figure 14. PCA for AR Coefficients of Separate Sensor and Actuator Circuit

In the control limit method, the AR model is compared to the incoming experimental data. When the error falls significantly above the accepted outliers per data point metric, then it will be flagged as damage. Within this paper, the control interval method is used as an unsupervised method for damage detection. In Figure 15, the error between the experimental data and the AR model is plotted, along with the associated control limits. It is clearly distinguishable that Figure 15 (a), which is for the undamaged structure, displays less error outliers than Figure 15 (b), the damaged structure.

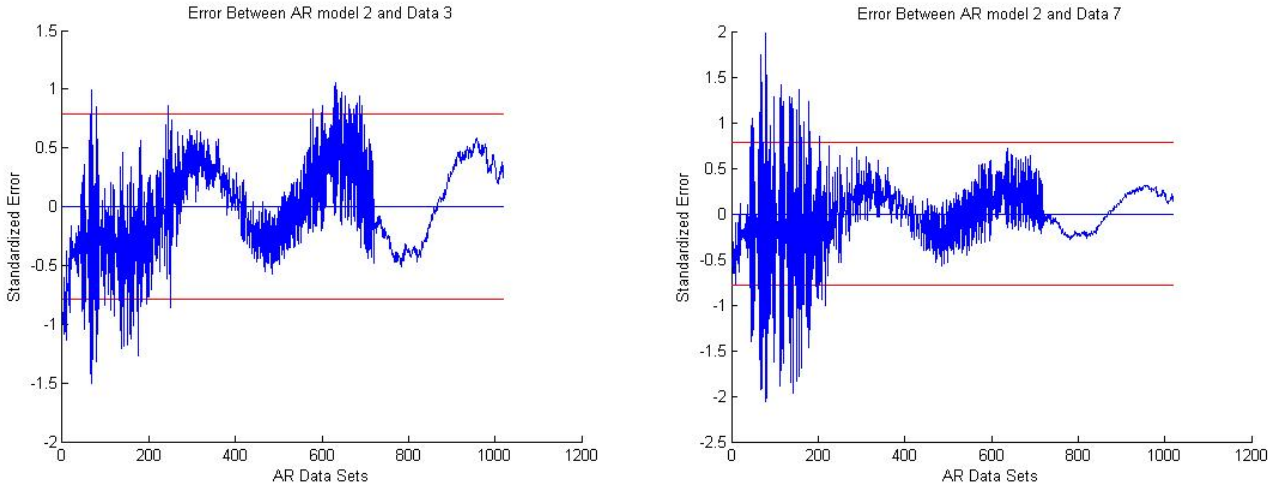

(a) (b)

Figure 15. Outlier Error between AR Model and Experimental Data (a) Undamaged Structure (b) Damaged Structure

Vector methods were also used to determine the correlation between either time data or frequency data. For time data that is triggered consistently, when the dot product of the normalized amplitude data is taken, the undamaged data has a value from 0.9 to 1.0, while the damaged data has a value around 0.1 to 0.0. In Figure 16 (a), when the time series data for Test 3 is compared to all 7 tests, Test 6 and 7 have a value close to one which indicates poor correlation. When Test 7 is compared in Figure 16 (b), the undamaged cases all have poor correlation. For frequency data, the vector methods are more effective at detecting the damaged structure than vector methods with time. In Figure 17 (a), Test 3 is compared to all 7 tests, and in Figure 17 (b), Test 7 is compared to all 7 tests. The values for damaged structures is effectively 1, while undamaged was effectively 0.

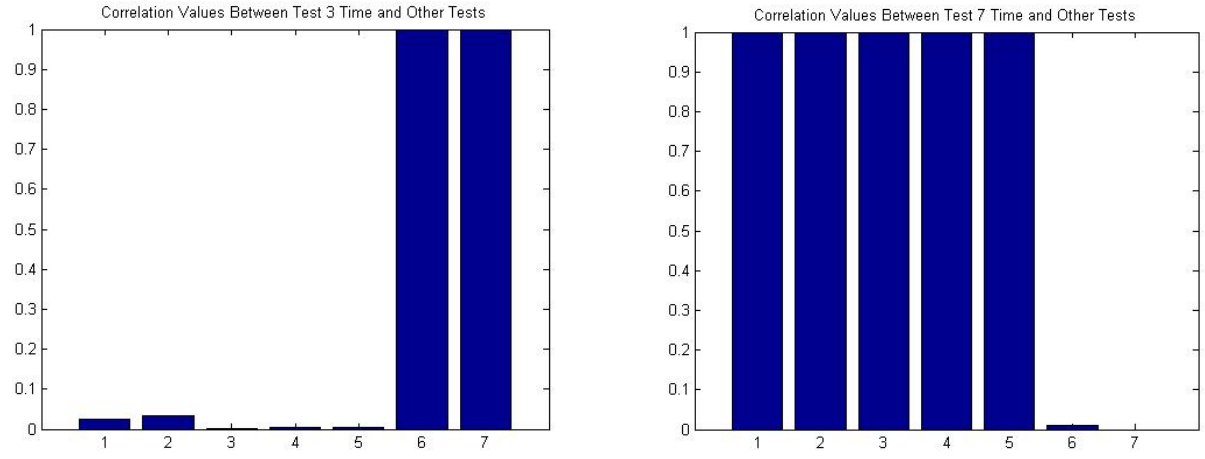

(a) (b)

Figure 16. (a) Test 3 Time Correlation (b) Test 7 Time Correlation

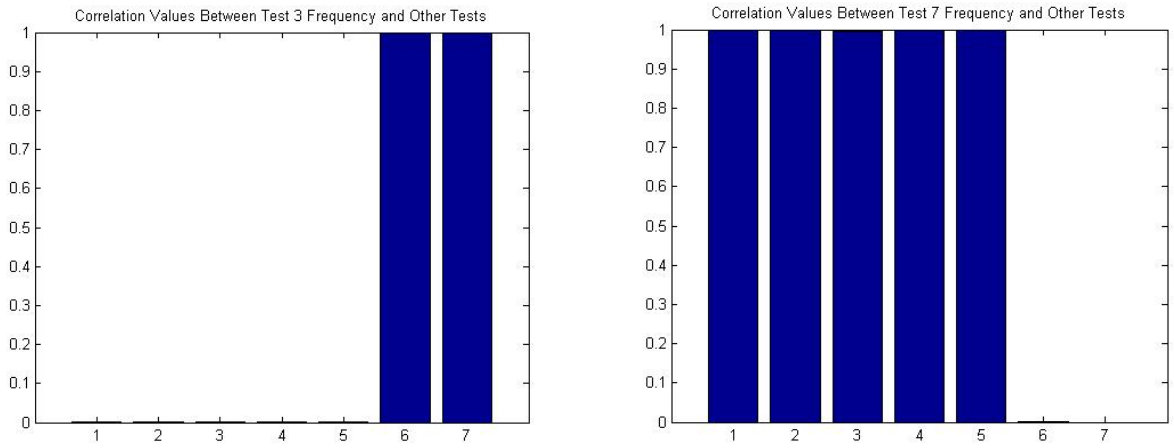

(a) (b)

Figure 17. (a) Test 3 Frequency Correlation (b) Test 7 Frequency Correlation

To validate the efficiency of the proposed damage detection methods, a three story frame structure is used as a test setup for detecting and locating damage. Constructed of unistrut columns and aluminum floor plates, the dimensions of the frame structure are displayed in Figure 18 [11]: where the aluminum floor plates are 0.5 inches thick and are attached to the unistrut columns with two bolts and one angled bracket. The test setup is supported on four Firestone airmount isolators. However, these isolators were previously integrated into the test setup, as their function was not intended for translational and torsional motion.

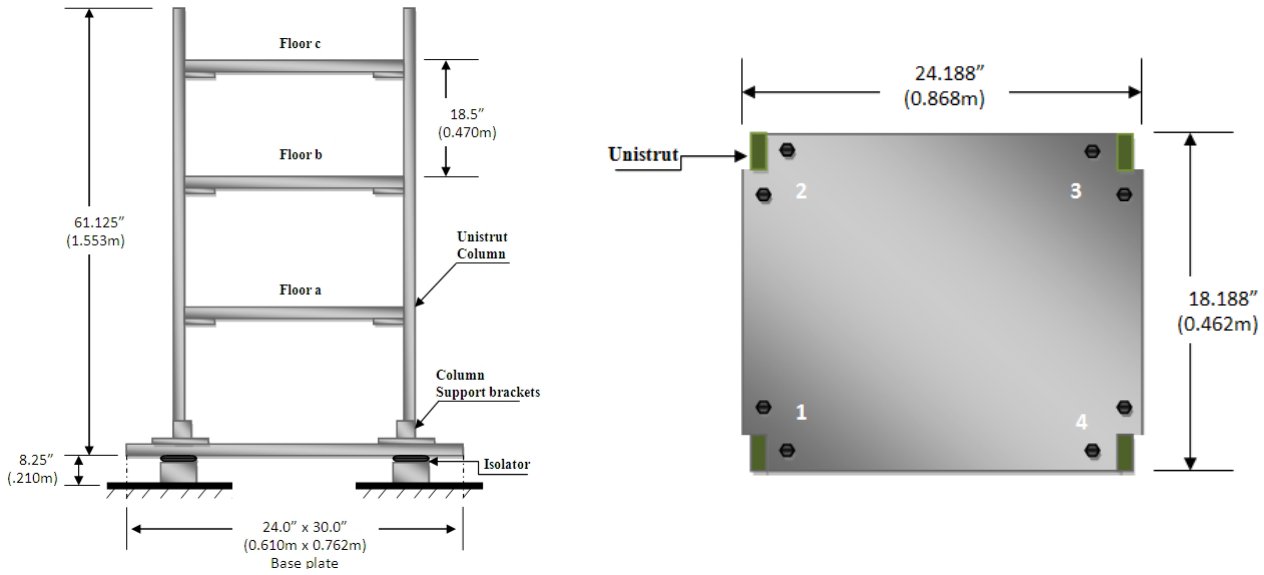

(a) (b)

Figure 18. Three Story Frame Structure (a) Structure Side View (b) Top View of Floor

With the aforementioned test structure, PZT patches were placed on the structure joints. As seen in Figure 19 (a), four PZT patches are positioned on the structure, where two patches are located on Floor b (Patch 5 and 4) and other two patches are placed on Floor C (Patch 2 and 3). The following table lists the measured patch capacitances.

Patch Capacitance	
Patch 2	3.25 nF
Patch 3	3.22 nF
Patch 4	3.38 nF
Patch 5	3.18 nF
External Patch (C_2)	4.49 nF

Table 7 Capacitance Values of PZT Patches

Damage was implemented to the structure by removing a single bolted connection, which is indicated in Figure 19 (b), on Floor b and at location Patch 5.

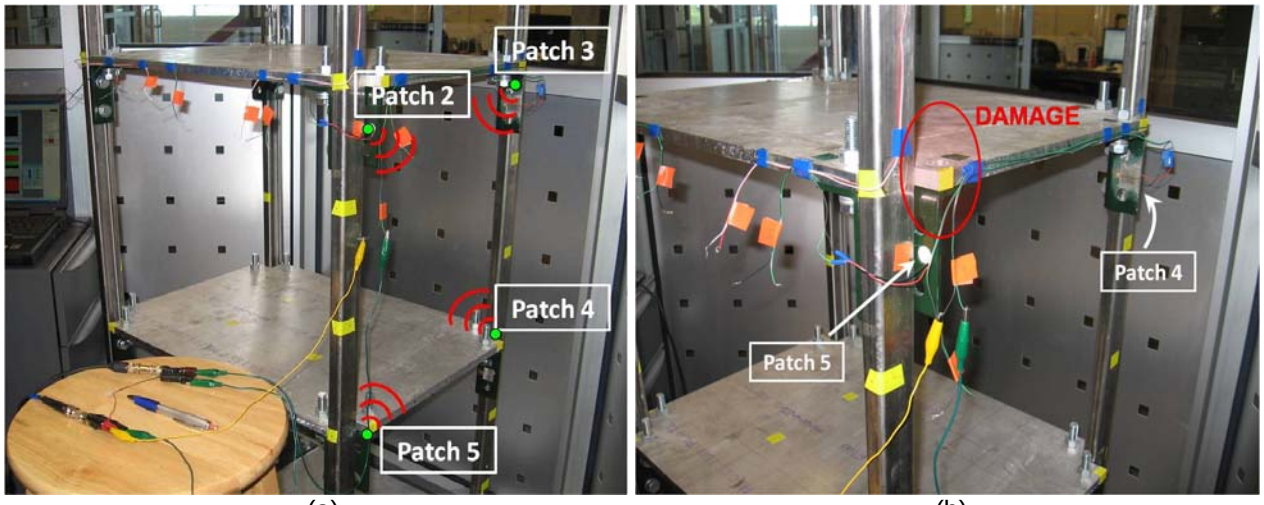

(a) (b)

Figure 19. Three Story Frame Structure (a) PZT Patch Locations (b) Damage Location at Patch 5

To assess damage localization, un-scaled correlation coefficients of the FRFs were evaluated between the damaged and undamaged structure. Twenty experimental tests were obtained, where the first ten tests consist of the undamaged structure and the second half of the damaged structure tests. In looking at Figure 20, there is a clear indication of damage being located at Patch 5. Patch 4 also denotes a low damage level. However, this effect is inherently due to the location of Patch 4, as it is attached to the same aluminum floor beam as Patch 5.

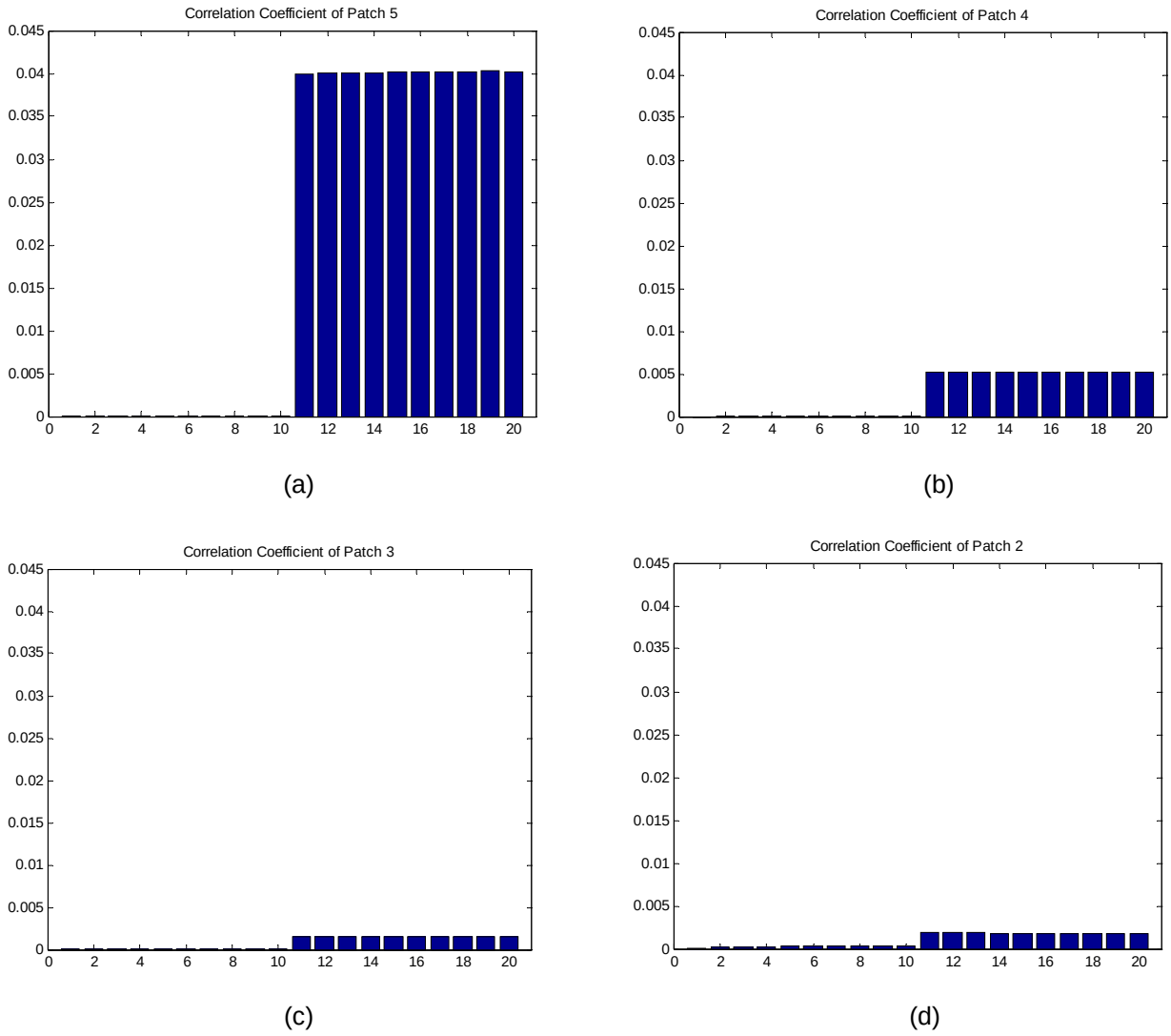

Figure 20. FRF Correlation Coefficients for Damage Detection and Localization (a) Patch 5 (b) Patch 4 (c) Patch 3 (d) Patch 2

5.2 SHM WITH SELF-SENSING ACTUATOR

In monitoring structural health, PCA methodology is utilized for the collocated self-sensor actuator, which is similar to the analysis previously conducted for the separate sensor and actuator. For the plot in Figure 21, the 4^{th} order AR model is used, where the input waveform is a shaped random input. As seen in Figure 21, there is a clear dividing line between the undamaged cases, the circles, and the damaged cases, the crosses.

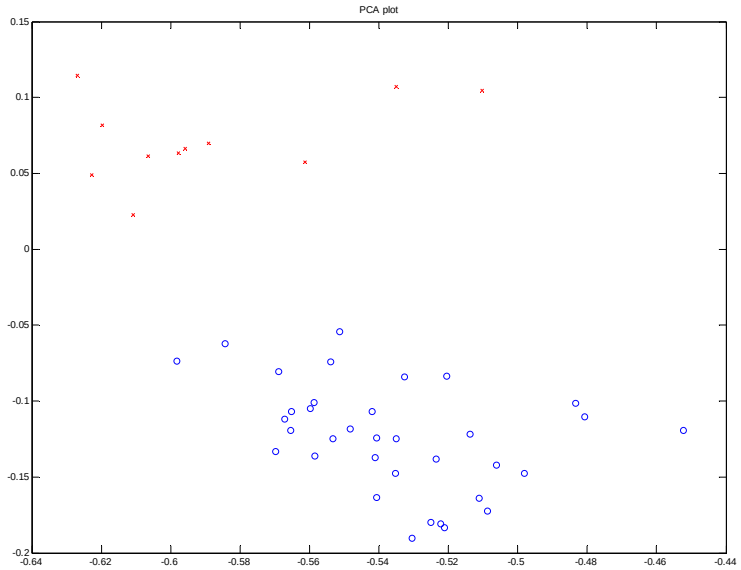

Figure 21. PCA for AR Coefficients of Self-Sensing Circuit

6.0 STRUCTURAL HEALTH MONITORING AND VIBRATION CONTROL

In order to verify that both tasks can be accomplished using the self sensor on the cantilevered beam, vibration reduction was tested with the SHM signal running, then SHM was tested with the vibration control running. The self sensor results were compared with the separate sensor and actuator results to verify that the performance. Damage was induced by placing a 2 g. piece of silicone putty on the beam to increase damping. In Figure 22, the putty used to simulate damage in the combined SHM and vibration suppression tests is located near the cantilevered beam base. For the self sensor case, the top patch was used as the self sensing actuator. For the separate sensor actuator tests, the top patch was used as a sensor and the bottom patch, which is not pictured, was used as the actuator.

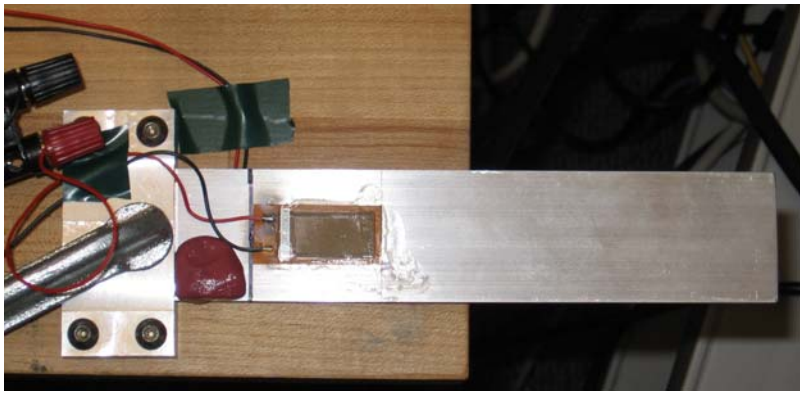

Figure 22. MFC Beam with Simulated Lump Mass Damage

6.1 VIBRATION SUPPRESION PERFORMANCE WITH SHM SIGNAL ON

The effect of the SHM signal on the vibration suppression performance is negligible. Figure 23 (a) shows the control performance with the SHM signal on while Figure 23 (b) shows the control performance with the SHM signal off. Both signals are from the separate sensor and actuator configuration. With the SHM on, the settling

time is 0.71 seconds, whereas with SHM off, the settling time is 0.52 seconds. When this settling time is compared to the 1.72 seconds for the uncontrolled signal, the 0.2 seconds difference is noticeably small.

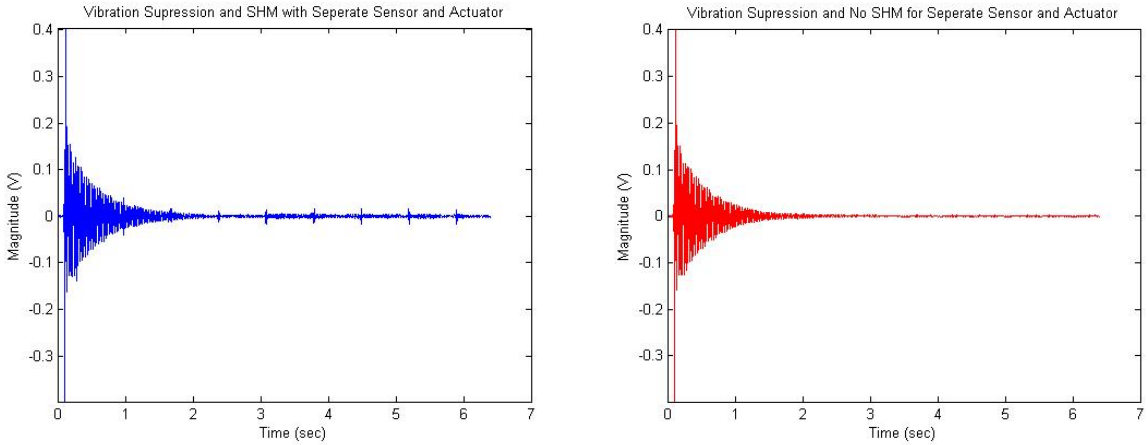

(a) (b)

Figure 23. Experimental Vibration Control of Separate Sensor and Actuator (a) SHM On (b) SHM Off

The self-sensor control performance when the SHM signal is on is nearly identical to when the SHM signal is off. The settling time for SHM on is 0.0688 seconds, and 0.0687 seconds for the SHM off case. The high frequency sine sweep produces no change in performance. The uncontrolled output settling time was 0.7672 seconds, which is significantly greater than the controlled case. Figure 24 (a) shows vibration suppression with the SHM on, while Figure 24 (b) shows vibration suppression with the SHM off. The impulse given to the self-sensor was 40% the separate sensor and actuator magnitude, which was attributed to the operational amplifiers voltage limits.

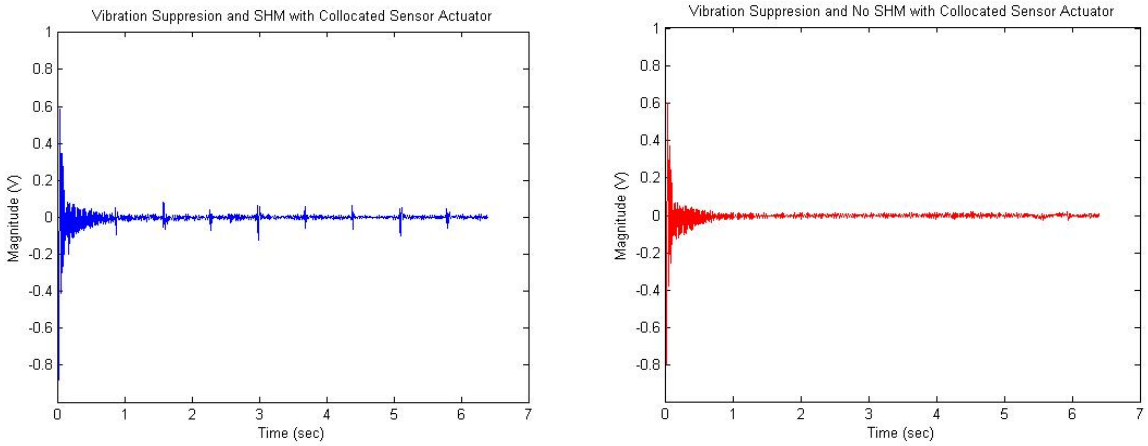

(a) (b)

Figure 24. Experimental Vibration Control of Collocated Sensor and Actuator (a) SHM On (b) SHM Off

6.2 SHM PERFORMANCE WITH VIBRATION CONTROL SIGNAL ON

SHM is possible while the vibration control signal is on, though there are several special precautions that need to be implemented to ensure data quality. To improve the SHM performance in the frequency domain, the data must be compared over the frequency range the structure was excited. The varying low frequency amplitudes distort the FRF and make the SHM vector methods less clear. Due to the much smaller SHM signal amplitude in comparison to the vibration suppression signal, the time domain data is improved by a high pass filter. When the

filter is not applied, data with vibration control cannot be compared to data without, since the low frequency signal dominates the AR model.

By choosing the analysis frequency range, it is clear in Figure 25 that choosing the range provides a more reliable identifier than using the full frequency range. In Figure 25 (a), the FRFs are compared across the full frequency range of 0 Hz to 20 kHz. It is noticeable that the correlation is weak for Test 5, which corresponds to a damaged case. In Figure 25 (b), the FRFs are compared across the excitation frequency range of 9 kHz to 12.5 kHz. All of the undamaged structures have significantly low values while the damaged cases appear closer to 1.0. The low value in Test 5 is largely eliminated by the focused approach.

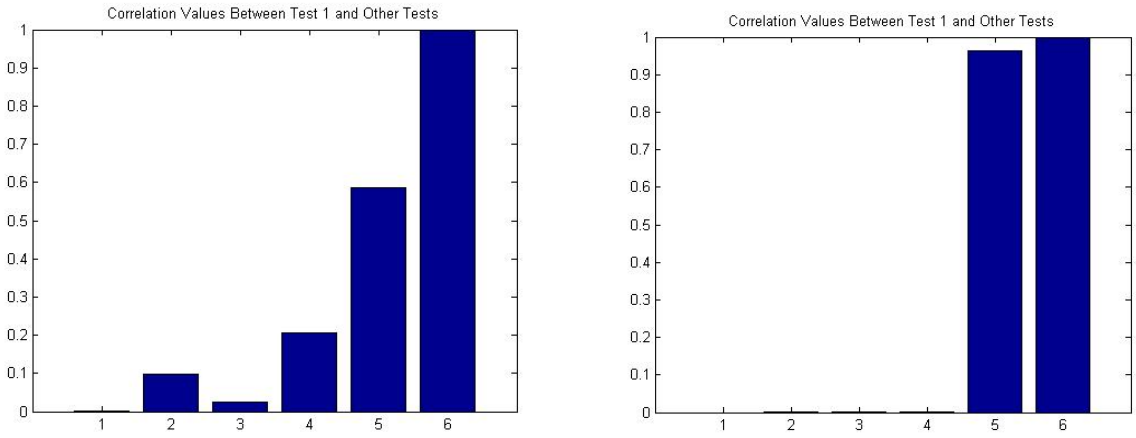

(a) (b)

Figure 25. FRF SHM using Vector Methods (a) Over Full Range (b) Over Excitation Range

By choosing the analysis frequency range, it is clear in Figure 26 that choosing the range provides a better identifier than using the full frequency range. In Figure 26 (a), the FRFs are compared across the full frequency range of 0 Hz to 20 kHz, and the correlation is weak for test 5, a damaged case. In Figure 26 (b), the FRFs are compared across the excitation frequency range of 9 kHz to 12.5 kHz. All of the undamaged structures have very low values while the damaged have high. The lower values of the last 5 tests are largely eliminated by the focused approach.

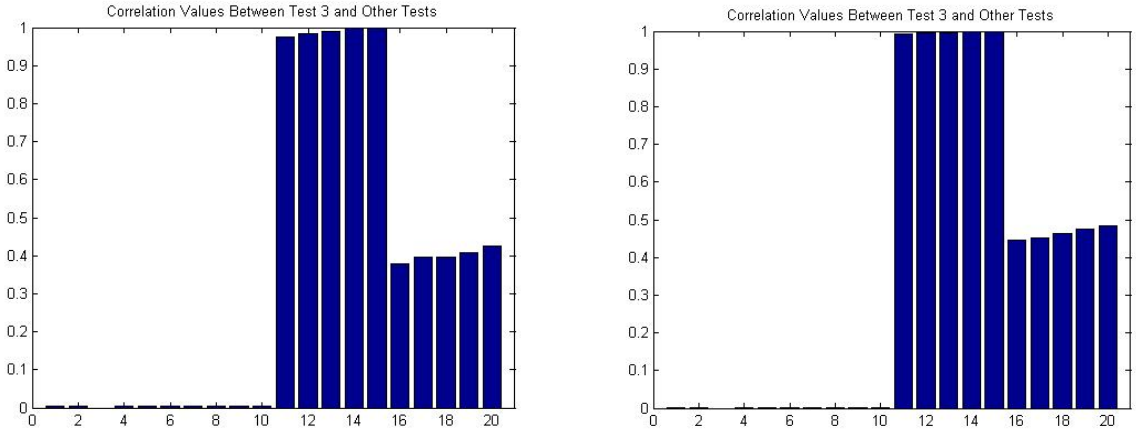

(a) (b)

Figure 26. FRF SHM using Vector Methods on Collocated Sensor Actuator (a) Over Full Range (b) Over Excitation Range

The time based SHM methods were not very effective when the Vibration Control signal was on. Time based methods are very sensitive to low frequency inputs, like operation vibrations and the control signal. Frequency methods have several advantages over time methods, FRFs are averaged, whereas time data is a single measurement. FRFs incorporate both the response input and output data, where the AR model only looks at the output. The FRFs can be analyzed without low frequency components. A high pass filter would need to be implemented to remove this interference from the time signal, and one was not available when the time series data was taken.

7.0 CONCLUSION

To efficiently suppress vibrations within a structure, a bridge circuit was implemented into the overall system, where techniques of increasing the bridge circuit temperature stability were also verified. The circuit used in SHM was simplified to reduce the frequency dependence. Vibration suppression was implemented using a separate sensor and actuator system, and a collocated sensor actuator with acceptable performance in both cases. SHM was implemented in both systems, with frequency methods effectively detecting damage, and time domain methods giving a small number of false positives. Vibration suppression was discovered to be insensitive to the SHM signal. SHM frequency domain methods are immune to vibration control signals and SHM time domain methods currently are not. Further research is required to isolate time domain SHM methods from the vibration control signal. Experimentally, it is essential for the improved self sensor concept to be verified that it does increase temperature stability.

ACKNOWLEDGEMENTS

This group would like to thank the Los Alamos Dynamics Summer School for the resources to conduct this project.

The following companies donated software:

The Mathworks, Inc. (MATLAB)
SIMULIA Americas (ABAQUS)
Vibrant Technology Inc. (MEScope)

REFERENCES

[1] E. F. Crawley and J. de Luis. 1987. “Use of Piezoelectric Actuators as Elements of Intelligent Structures,” *AIAA Journal*, Vol. 25, Iss. 10, pp.1373-1385.

[2] J.L. Fanson and T.K. Caughey. 1990. “Positive Position Feedback Control of Large Space Structures,” *AIAA Journal*, Vol. 28, Iss. 4, pp. 717-724.

[3] J. Dosch, D.J. Inman and E. Garcia, 1992, “A Self-Sensing Piezoelectric Actuator for Collocated Control,” *Journal of Intelligent Material Systems and Structures*, Vol. 3, pp. 116-185.

[4] J. Tani, G.G. Cheng, and J. Qiu. 1997. “Effectiveness and Limits of Self-Sensing Piezoelectric Actuator,” *Proceedings of First Structural Health Monitoring Workshop, Stanford, CA.* Vol. 1, pp. 502-514.

[5] M. Okugawa and M. Sasaki. 2002. “System Identification and Controller Design of a Self-Sensing Piezoelectric Cantilever Structure,” *Journal of Intelligent Material Systems and Structures, Vol. 13, Iss.4, pp. 241-252.*

[6] G.E. Simmers Jr., J.R. Hodgkins, D.D. Mascarenas, G. Park and H. Sohn, 2004, “Improved Piezoelectric Self-sensing Actuation,” *Journal of Intelligent Material Systems and Structures*, Vol. 15, pp. 941-953.

[7] J.S. Vipperman and R.L. Clark. 1996. “Implementation of an Adaptive Piezoelectric Sensor Actuator,”

AIAA Journal, Vol 34, pp. 2102-2109.

[8] D.M. Castillo, C. Pardo de Vera and J.A. Guemes. 1999. “Structural Integrity Analysis with Piezoelectric Patches,” *Key Engineering Materials. Vol.* 167, pp. 91-101.

[9] Z.A. Chaudhry, T. Joseph, F.P. Sun, and C.A. Rogers. 1995. “Local-Area Health Monitoring of Aircraft Via Piezoelectric Actuator/Sensor Patches,” *SPIE*, Vol. 2443 pp. 268-276.

[10] G. Park, H. Sohn, C.R. Farrar and D.J. Inman. 2003. “Overview of Piezoelectric Impedance-Based Health Monitoring and Path Forward,” *The Shock and Vibration Digest*, Vol. 35, No. 6, pp. 451-463.

[11] T. Fasel, H. Sohn, and C.R. Farrar. 2003. “Damage Detection Using Frequency Domain ARX Models and Extreme Value Statistics,” *The 21st International Modal Analysis Conference*, Kissimmee, FL, USA, Feb. 3-6.